

Nitric-oxide-feedback to ciliary photoreceptor cells orchestrates UV avoidance in zooplankton

Kei Jokura, Nobuo Ueda, Martin Gühmann, Luis Alfonso Yañez-Guerra, Piotr Słowiński, Kyle C. A. Wedgwood, Gáspár Jékely

Living Systems Institute, University of Exeter, Stocker road, Exeter, EX4 4QD, UK

Abstract

Nitric oxide (NO) generated by nitric-oxide synthase (NOS) is a key regulator of animal physiology. Here we uncover a role for NO in shaping circuit dynamics to orchestrate light-avoidance behaviour. We studied UV-avoidance mediated by brain ciliary photoreceptors (cPRCs) in larval *Platynereis dumerilii*, a marine annelid. We found NOS specifically expressed in interneurons (INNOS) postsynaptic to cPRCs. Stimulation of cPRCs by violet light leads to cPRC inhibition but concomitant INNOS activation and NO production. NO feeds back to cPRCs and triggers their delayed activation through an unconventional guanylyl cyclase. This results in the activation of projection interneurons and the inhibition of serotonergic ciliomotor neurons. In NOS mutants, NO feedback and projection-neuron activation do not occur and avoidance behaviour is defective. By mathematical modelling, we could capture the circuit dynamics in both wild-type and mutant larvae. Our results reveal how NO-mediated neuroendocrine signalling gates a synaptic circuit to initiate light-avoidance behaviour.

Introduction

The ability to perceive changes in the environment and adapt behaviour accordingly is essential for the survival of all living organisms. Avoidance from UV radiation, which damages DNA essential for survival, is proposed to be one of the behaviours that existed before the abundant development of Earth's oxygen to block UV radiation in the atmosphere (Pittendrigh). In the ocean, almost all zooplankton have a pronounced rhythmic behaviour called Diel vertical migration (DVM), which consists of upwards towards the surface at dusk and descend back to deeper water before dawn. Avoidance behaviour to escape harmful UV radiation during the day is closely linked to the control of vertical migration in the ocean. However, little is known about the molecular neural circuit mechanisms in UV avoidance behaviour in many animals, including zooplankton. In neural circuits in general light response, the activation of various receptors by excitatory and inhibitory neurotransmitters such as glutamate, GABA and dopamine is known in various species. In addition to this, it has long been known that in nitric oxide (NO), as a neuromodulatory molecule, it is also important as a modulator of visual activity. NO is a small free-radical molecule with diffusible and changeable characteristics, and thus works as one of the neural signalling molecules. The function of NO in the neural circuitry of vision has been well studied in vertebrates. In the mammalian retina, NO is an essential signalling molecule in all retinal cells. NO produced by nitric oxide synthase (NOS) in amacrine cells, one of the retinal cells, activates soluble guanylate cyclase (sGC) expressed in cone bipolar cells, which produces cGMP and regulates downstream signalling. We therefore hypothesise that NO-mediated neural signalling may be involved in the photoreceptor circuits that control UV avoidance behaviour. To test this hypothesis we used the annelid *Platynereis dumerilii* (**Figure 1A**), which conserved vertebrate-type ciliary photoreceptors (cPRCs) (Arendt et al., 2004). The cPRC expresses *c-opsin1*, which absorbs UV radiation, is involved in melatonin production and regulates circadian swimming behaviour (Tosches et al., 2014; Tsukamoto et al., 2017). Furthermore, we previously reported abnormal UV avoidance behaviour in *c-opsin1* knockout larvae (Verasztó et al., 2018). The cPRCs express the UV-absorbing *c-opsin1* and mediate UV avoidance in the larvae (Verasztó et al., 2018). In adult worms, UV light and *c-opsin1* modulate locomotion and maturation (Veedin Rajan et al., 2021). These suggest that *Platynereis* larvae

are a highly suitable model for elucidating the neural circuit mechanisms of NO-induced UV avoidance behaviour, and the accessibility of genome editing, behavioural assays, calcium imaging and whole-body connectomics could be very useful for study at the molecular level(Ozpolat et al., 2021).

Results

Nitric oxide synthase is expressed in interneurons of the UV-avoidance circuit

We identified a single *nitric oxide synthase* (*NOS*) gene in the *Platynereis dumerilii* genome and transcriptome data. Phylogenetic analysis of NOS proteins indicate that *Platynereis* NOS belongs to an orthology group of metazoan NOS sequences (**Figure 1—figure supplement 1**). To characterise the expression pattern of *NOS* we used *in situ* hybridization chain reaction (HCR) and transient transgenesis. In two- and three-day-old larvae, we detected *NOS* expression in four cells (two of them weakly expressing) in the apical organ region (**Figure 1D** and **Figure 1—figure supplement 2**). The same four cells were labelled with a reporter construct driving palmitoylated-tdTOMato by a 12 kbp upstream genomic region of the *NOS* gene (**Figure 1E**). This reporter also revealed the axonal projections of the NOS-expressing neurons. The position and morphology of the four *NOS*-expressing cells allowed us to identify the same cells in the three-day-old whole-body volume EM data (Verasztó et al., 2020; Williams et al., 2017) as four interneurons (INNOS) (**Figure 1B,C**). The INNOS cells are postsynaptic to the UV-sensory cPRCs and presynaptic to the INRGW interneurons, which are also cPRC targets (**Figure 1C,F**). INRGW neurons synapse on the head serotonergic ciliomotor neurons (Ser-h1), which synapse on the prototroch ciliary band and the cholinergic MC ciliomotor neurons (**Figure 1C,F**). We also detected *NOS* expression by HCR in the region of the visual eyes (adult eyes) and the pigmented eyespots (**Figure 1—figure supplement 1**).

Nitric oxide produced during UV/violet stimulation gates the output of the cPRC circuit

The specific expression of *NOS* in interneurons directly postsynaptic to the cPRCs suggests that NO signalling is involved in the UV response. To test if NO is produced during UV/violet responses, we injected zygotes with the fluorescent NO-reporter DAF-FM and imaged two-day-old larvae during the local stimulation of the cPRC cilia by 405 nm light. Following light stimulation, we detected an increase in DAF-FM fluorescence in the region of the INNOS cells (**Figure 2**).

Nitric oxide signalling mediates UV-avoidance behaviour

To test this, we generated two *Platynereis* *NOS* knockout lines with the CRISPR/Cas9 method. We recovered two deletions (*NOS* Δ 11/ Δ 11 and Δ 23/ Δ 23), both leading to an early stop codon and thus likely representing null alleles (**Figure 3A**). We could establish a homozygous line for both mutations indicating that *NOS* is not an essential gene. To quantify UV avoidance, we recorded the trajectories of freely swimming larvae in vertical columns, illuminated laterally from two opposite sides with 395 nm UV/violet light. To analyse the behaviour of larvae before and after UV stimulation, the temporal changes in some parameters were compared using tracking of individual larvae of the WT and mutant (**Figure 3B,C** and **Figure 3—figure supplement 1A-D**). The results showed that in the WT there was a rapid and strong increase in downward swimming approximately 15 s after UV stimulation, whereas this did not occur in the mutant (**Figure 3C** and **Figure 3—figure supplement 1B**). Interestingly, there was already a difference in swimming speed between the WT and the mutant before UV stimulation (in the dark) (**Figure 3—figure supplement 1C,D**). After UV stimulation, the swimming speed of the WT increased and reached a maximum after about 20 s. In contrast, the mutants showed a slight increase in speed after UV stimulation, but swimming speed was not maintained and returned to the speed before UV stimulation. We also tested phototaxis, by exposing larvae to 480 nm directional and collimated light from the top of the column. As previously shown, wild-type larvae swim downward within 30 sec following non-directional UV/violet light stimulation (Verasztó et al., 2018). In contrast, homozygous *NOS*-mutant larvae showed a strongly diminished UV-avoidance response (**Figure 3D** and **Figure 3—figure supplement 1E**). This phenotype is similar to the defective UV-avoidance of *c-opsin1* mutant larvae and reveals a requirement for *NOS* in UV-avoidance behaviour (Verasztó et al., 2018). *NOS*-mutant larvae also showed reduced phototactic behaviour, suggesting a function in the visual eyes mediating phototaxis (Randel et al., 2014).

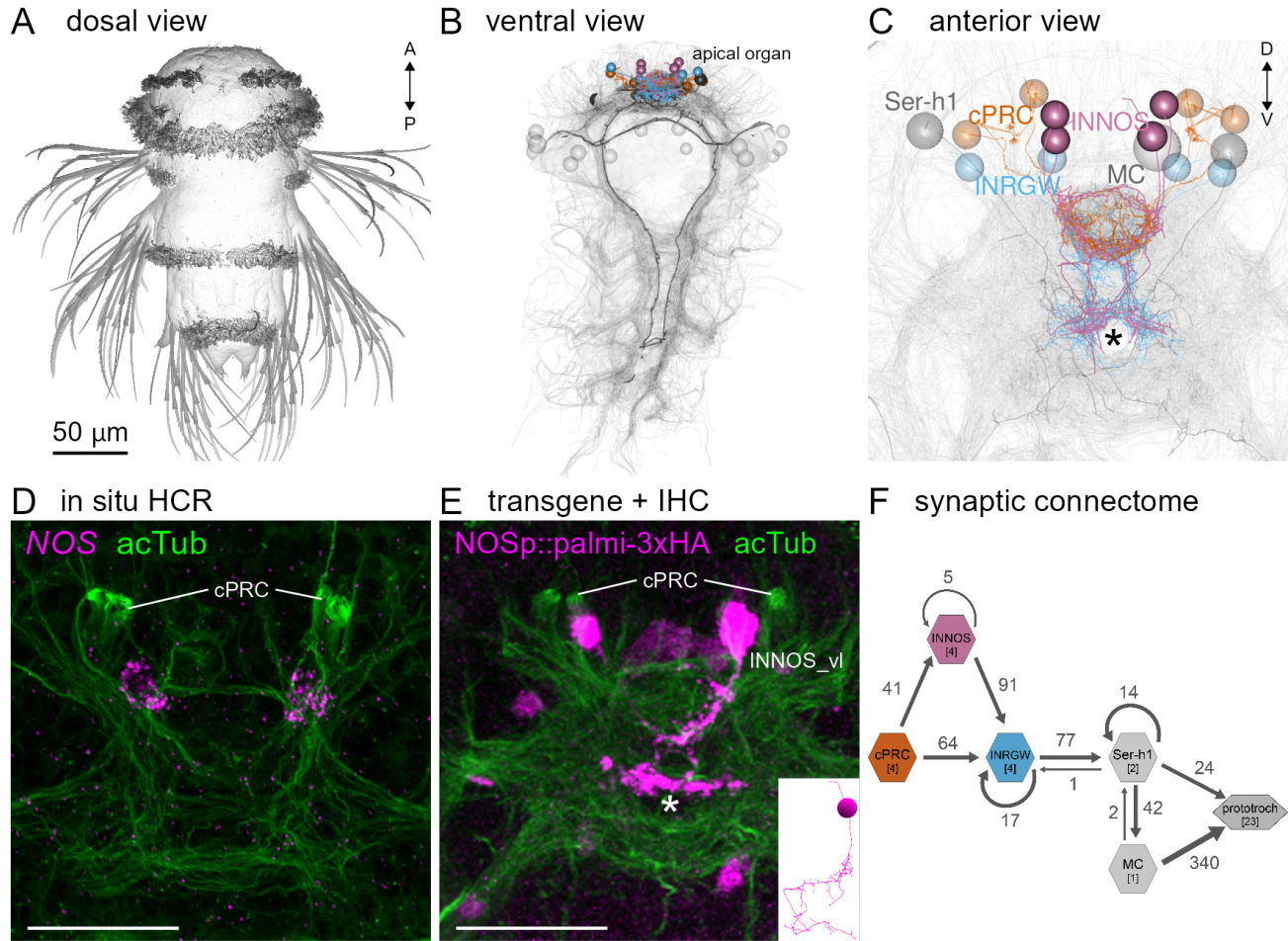


Figure 1: Figure 1. Identification of NOS-expressing interneurons (INNOS) within the cPRC circuit. **(A)** SEM image of a three-day-old Platynereis larva. **(B, C)** Five types of neurons (cPRC, INNOS, INRGW, Ser-h1 and MC) in the cPRC circuit reconstructed in the whole-body transmission electron microscopy (ssTEM) dataset of a three-day-old larva. Ciliated cells labelled with (B) are shown in grey. The INNOS on the ventral side labelled with (C) are shown in purple. Axons and dendrites appear as lines and cell body positions are represented by spheres. **(D)** Expression analysis of the NOS gene (magenta) using in situ HCR. Anterior view of the larva at two-day-old. Co-stained image using acetylated α -tubulin antibody (actub: green). **(E)** Immunostaining with anti-HA antibody against HA tagged palmitoylated-tdTomato expressed under the upstream of the start site of NOS (NOSp::palmi-3xHA: magenta). Co-staining with acetylated α -tubulin antibody as marker for cilia of cPRC and axonal scaffold (actub: green). Views of larvae at three-day-old from the anterior side. Insert: One of the reconstructed INNOS is shown from the anterior side. **(F)** Wiring diagram of the cPRC circuit. Hexagons and arrows represent cell groups and their synaptic connections, respectively. Numbers inside hexagons indicate the number of cells grouped in each node. Arrow line thickness (synapse weight) is equal to the number of synapses.

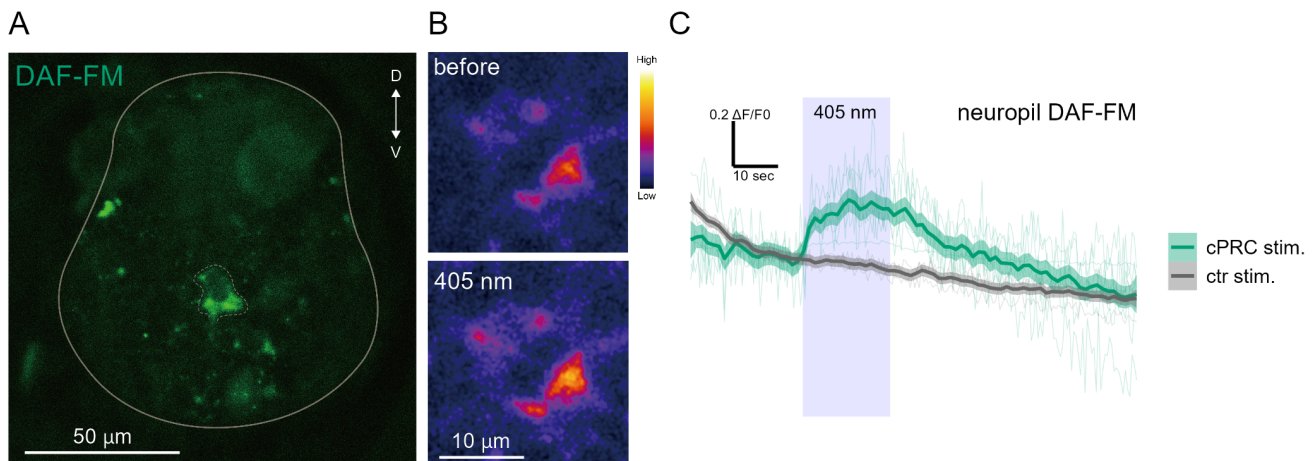


Figure 2: Figure 2. NO produced by UV/violet stimulation to cPRCs. (A) A NO-positive cell visualised by DAF-FM (green) is shown (dashline). The white line indicates the outer frame of the larva. All subsequent images are of two-day-old larvae. (B) Intensity changes before (upper) and during 405 nm light stimulation (lower) in a cell visualised by DAF-FM. (C) The intensity of DAF-FM changes over time when cPRC (green) and other cells (ctr: gray) are stimulated with UV/violet (405 nm) light. Purple squares indicate the timing of 405 nm light stimulation, the transparent lines show the optical responses to individual intensities, each intensities are normalized ($\Delta F/F_0$) and the dark trace lines and the shaded bands show the mean value and the standard error range of the mean.

where NOS is also expressed (Figure 1—figure supplement 1A,B). To test if the observed defects are due to a role of NOS in neuronal signalling or circuit developmental, we also tested larvae exposed to a NOS inhibitor, L-NAME. Larvae incubated for 5 min in 0.1 mM or 1 mM L-NAME showed defective UV avoidance, but normal phototaxis (Figure 3E). Overall, our results indicate an acute requirement for NOS signalling in UV-avoidance and a possible indirect, developmental role in the visual system. To investigate the role of NO on UV avoidance behaviour, receptors for NO were explored.

Two unconventional guanylyl cyclases are expressed in the cPRCs

NO generally acts via soluble guanylate cyclases (sGC), belonging to the guanylate cyclase family with a CYC domain (PF00211). NO binding to the heme group of sGC leads to increased cyclic guanosine monophosphate (cGMP) production. Analysis of sGCs in *Platynereis* indicated that these genes are not expressed in any of the cells of the cPRC circuit (Verasztó et al., 2017). Recently, Moroz and coworkers reported an atypical but widely conserved family of guanylyl cyclases with a NIT (nitrite/nitrate sensing) domain (PF08376) (NIT-GC)(Monteagudo-Cascales et al., 2023; Shu et al., 2003) as potential mediators of NO signalling (Moroz et al., 2020). To search for NIT-GCs in *Platynereis*, we searched transcriptome resources and retrieved 15 potential NIT-GC homologs (Figure 4—figure supplement 1). To analyse the relationship of these sequences to metazoan NIT-GCs, we retrieved protein sequences with a CYC domain from the transcriptome and genome databases of 45 metazoan species and 2 choanoflagellate species. We carried out cluster analysis and did phylogenetic reconstruction on a group of membrane-bound guanylyl cyclases with sGCs as an outgroup. In agreement with Moroz et al. (Moroz et al., 2020), we found a group of GCs with NIT domains with representatives in placozoans, cnidarians, some ecdysozoans, echinoderms, and lophotrochozoans. The 15 *Platynereis* sequences were parts of several major and ancient clades of the tree (Figure 4—figure supplement 1). To characterise the expression of NIT-GCs, we used previously published spatially mapped single-cell transcriptome data (Achim et al., 2015; Williams et al., 2017). Among the 15 NIT-GCs, two showed high and specific expression in the cPRCs and one was expressed in the INNOS cells (Figure 4—figure supplement 1). In the single-cell data, we could identify the cPRCs by the specific expression of c-opsin1 and a pedal-peptide2 neuropeptide precursor (MLD proneuropeptide) (Arendt et al., 2004; Williams et al., 2017), which have previously been described as cPRC markers (Figure 4—figure supplement 2A).

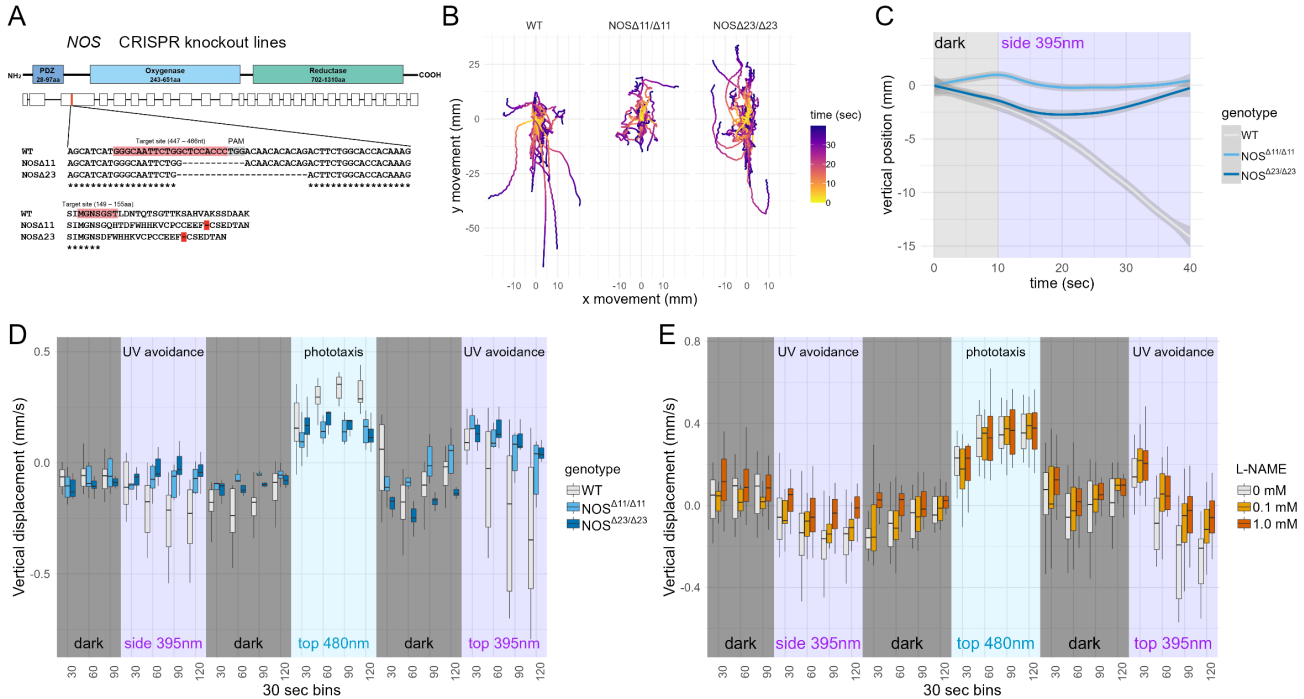


Figure 3: Figure 3. Larvae with inhibited NOS have a delayed response to UV-avoidance. **(A)** Top: The domain and Exon/Intron structure of NOS. Bottom: Close-up region showing the genomic locus of NOS gene and the wild-type sequence (WT) targeted by CRISPR/Cas9. The generated mutants (NOS Δ 11, NOS Δ 23) are also shown. Pink indicates target sites. Gray shows PAM sequences, red shows stop codons. **(B)** Overlaid trajectories for WT ($n=32$) and NOS mutant (NOS Δ 11/Δ11, $n=26$ and NOS Δ 23/Δ23, $n=47$) at three-day-old larvae. 0 sec as the starting point. After 10 sec, UV (395 nm) stimulation from the side. **(C)** The temporal changes in the vertical position of the WT and mutant larvae before (dark) and after UV stimulation (side 395 nm) are shown. The starting points of each larval trajectory are set to 0. **(D)** Vertical swimming in wild-type (WT) and mutant (NOS Δ 11 and NOS Δ 23) larvae at three-day-old stimulated with UV (395 nm) light from side, blue (488 nm) light from top and UV (395 nm) light from top. The data are shown in 30 s bins. **(E)** Vertical swimming in larvae treated with NOS inhibitor, L-NAME at three-day-old stimulated with UV (395 nm) light from side, blue (488 nm) light from top and UV (395 nm) light from top. The data are shown in 30 s bins.

The INNOS cells were identified by NOS expression and their spatial mapping. We decided to focus on two NIT-GCs expressed in the cPRCs and with a full-length sequences, NIT-GC1 and NIT-GC2. To confirm the single-cell data, we first carried out *in situ* HCR with probes for *NIT-GC1* and *NIT-GC2* mRNA. Both genes showed very clear and specific expression in the four cPRCs, as confirmed by co-labeling with an acetylated α-tubulin antibody and with an HCR probe against *MLD proneuropeptide* (**Figure 4A,B** and **Figure 4—figure supplement 2A-C**). To analyse the subcellular localisation of NIT-GC1 and NIT-GC2 at the protein level, we raised and affinity-purified polyclonal antibodies against a specific peptide sequence from both proteins. In immunostainings, we found that NIT-GC1 was localised to the region corresponding to the axonal projections of the cPRCs in the anterior nerve plexus (**Figure 4C**). Co-immunostaining with the rabbit NIT-GC1 and the rat NOS antibodies revealed that both proteins were localised in close proximity in the neurosecretory plexus (**Figure 4—figure supplement 2D**). In contrast, NIT-GC2 strongly and specifically labelled the large sensory ciliary region of the cPRCs (**Figure 4D**). These different subcellular localisations suggest that the two NIT-GCs are involved in different intracellular signalling processes in the ciliary and axonal regions of the cPRCs.

NIT-GC1 is required for the depolarising response of cPRC to UV stimulation

To investigate how NIT-GCs-mediated NO signalling is involved in cPRC activation, the calcium sensor GCaMP6s was ubiquitously expressed in larvae and calcium imaging in the cPRC during UV/violet stimulation. As we have shown previously, a 20-sec local stimulation of the ciliated part of the cPRC with 405 nm light lead to a transient decrease in cPRC calcium levels, likely due to the hyperpolarisation of the cPRCs (Verasztó et al., 2018). After 20-sec, calcium levels in cPRCs were raising again, reaching higher levels than at the start of the stimulus - a response that may involve depolarisation. This activation phase occurs after the end of the stimulation and may be due to a slower neuroendocrine feedback (Verasztó et al., 2018). First, to determine whether NO mediates such a feedback, we measured calcium levels in *NOS*-mutant larvae. While we detected the inhibition phase in cPRC in *NOS*-mutants, this was not followed by activation and calcium levels remained low (**Figure 4E,F**). These results revealed an essential requirement for NO signalling in the second phase of the cPRC response. Next, to characterise the role of NIT-GCs in changes of calcium levels in cPRC, calcium imaging was performed when each *NIT-GC* gene was knocked down using morpholino (**Figure 4—figure supplement 2E,F**). In NIT-GC1 morphant larvae, 405 nm light stimulation caused a decrease in calcium levels in the cPRC, but the increase in calcium levels that occurred after the light stimulation was stopped was strongly suppressed (**Figure 4G**). This result is similar to the response of *NOS* mutants in cPRC, suggesting that NIT-GC1 mediates depolarising responses after UV stimulation of cPRC by NO and may be involved in extracellular signalling. Interestingly, in NIT-GC2 morphant larvae, an increase in calcium levels occurred immediately after light stimulation (**Figure 4H**). The different responses of cPRC upon knockdown of NIT-GC1 and NIT-GC2 suggest that there may be different intracellular signalling mechanisms associated with their respective localisations. We focused our analysis on NIT-GC1 because it was localised to cPRC neuroaxons within the neuroplexas region and is involved in extracellular signalling after UV stimulation. It is generally known that depolarisation in the PRC involves elevated cGMPs in the photoreceptors. We therefore used an *in vitro* system in which cultured cells expressed NIT-GC1 to assess the cGMP activity of NIT-GC1.

NIT-GC1 produces cGMP by nitric oxide

NIT-GC1 has a highly conserved cyclase domain and activation of NIT-GC1 is expected to produce cGMP (**Figure 4I**). Recently, a synthetic protein called Green cGull was developed as a cGMP indicator that can be used in cultured cell systems (Matsuda et al., 2016). We co-expressed Green cGull and NIT-GC1 using the 2A self-cleaving peptide in cultured cells COS-7 (monkey kidney) and tested the intracellular dynamics of cGMP in the activation of NIT-GC1 (**Figure 4J**). When the NO donor SNAP was applied to the NIT-GC1 and Green cGull co-expression cells, the intracellular cGMP levels was significantly increased compared to when NIT-GC1 was not expressed (**Figure 4K,L**). The increase in fluorescence intensity also did not occur when DMSO was applied (**Figure 4M**). To confirm whether this increase in intracellular cGMP levels is NIT domain-dependent response of NIT-GC1, mutant form of NIT-GC1 without the NIT domain was expressed and SNAP was applied (**Figure 4I**). As a result, the increase in fluorescence intensity was significantly reduced (**Figure 4N**). These results indicate that NIT-GC1 produces cGMP

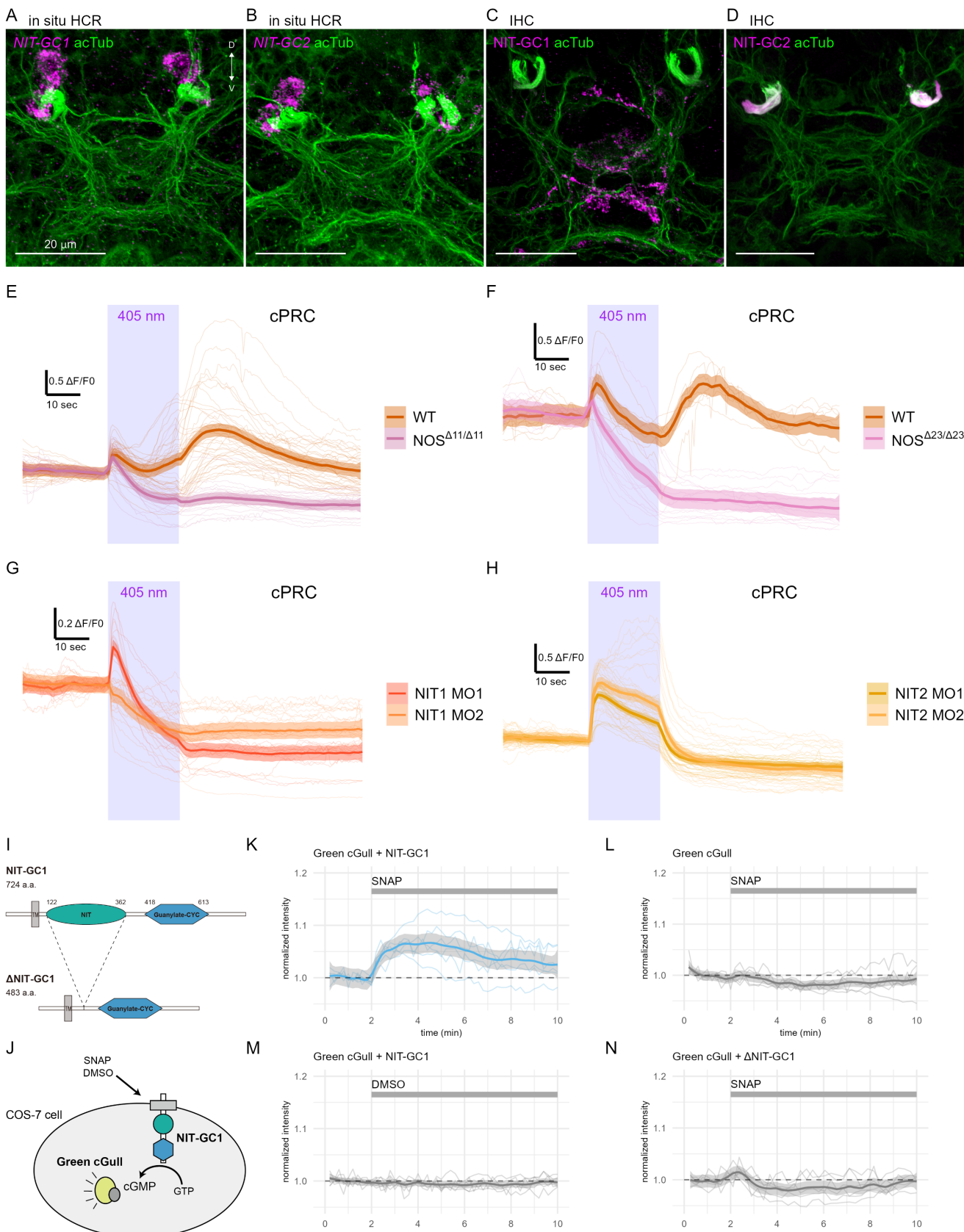


Figure 4: Figure 4. cPRC-specific expression of NIT-GC1 localises in close proximity to NOS in the ANS region. **(A, B)** Expression analysis of the NIT-GC1 (C) and NIT-GC2 (D) gene (magenta) using in situ HCR. Co-staining image using acetylated α -tubulin antibody (ac α -tub: green). **(C, D)** Localisation analysis using NIT-GC1 and NIT-GC2 antibodies. Green shows co-staining with acetylated α -tubulin antibody (ac α -tub). **(E, F)** Changes over time in GCaMP6s intensities in cPRC when stimulated with UV in WT (dark yellow) and NOS mutant (E: NOS Δ 11/ Δ 11, F: NOS Δ 23/ Δ 23) (light pink) larvae. **(G, H)** Changes over time in GCaMP6s intensities in cPRC when stimulated with UV in NIT-GC1 (G: NIT1) and NIT-GC2 (H: NIT2) knockdown by morpholino (MO1 and 2) larvae. **(I)**

via the NIT domain. In bacteria, it has been proposed that the NIT domain regulates cellular functions in response to changes in extracellular and intracellular nitrate and nitrite concentrations. Our results suggest that NIT-GC1 may be sensitive to NO. This could be a possible feedback pathway in which NIT-GC1 expressed in cPRC is activated by NO produced by INNOS. In order to further explore the role of NO in the cPRC circuit, we therefore compared calcium imaging of postsynaptic cells (INNOS, INRGW, Ser-h1 and MC) in the cPRC circuit during UV stimulation of cPRC between WT and NOS mutant larvae.

Depolarisation of cPRC is required for activation of downstream interneurons and ciliomotor neurons

We next quantified the responses of the INNOS and INRGW following a UV/violet stimulus to the cPRCs. To unambiguously identify the cells from which we recorded calcium signals, we developed an on-slide immunostaining method (**Figure 5—figure supplement 1**). We used the cell-specific neuropeptide markers using anti-RYamide (INNOS) and anti-RGWamide (INRGW) antibodies (Conzelmann et al., 2011) to mark the interneurons. Based on the position of the nuclei, we could correlate live and fixed samples at a single-cell precision (**Figure 5A,B**). In both wild-type and *NOS*-mutant larvae, INNOS cells showed increase calcium signals during the inhibition phase of the cPRCs (**Figure 5D**). In addition, INNOS depolarisation was suppressed in NIT-GC2 molphants where cPRC hyperpolarisation was suppressed (**Figure 5E**). This indicates that cPRC hyperpolarisation is required for INNOS depolarisation. In contrast, calcium signals increased in INRGW cells in wild-type larvae during the second activation phase of cPRCs, a response that was lacking in *NOS*-mutants (**Figure 5F,G**). This suggests that there is no circuit output to the Ser-h1 and MC cells and the ciliary band in *NOS*-mutants, consistent with the observed behavioural defects (**Figure 5H,I**).

Discussion

In the present study, we explored the role of NO in the UV avoidance behaviour of *Platynereis*. We demonstrated that there are interneurons expressing NOS in the cPRC circuit and that NO is required for UV avoidance in behavioural experiments using NOS mutants. We identified the axon-localised type NIT-GC1 and the cilia-localised type NIT-GC2 expressed in the cPRCs as targets of NO and showed from cultured cell experiments that these produce cGMP in response to NO. We have shown by calcium imaging that INNOSs are activated in response to the hyperpolarising response of the cPRCs, that the NO produced feeds back to the cPRC via NIT-GC1 and induces a depolarising response in the cPRC, and that the depolarising response of the cPRC is involved in activating downstream INRGW. Lastly, we confirmed that RGWamide induces the downward swimming behaviour of larvae.

cPRCs expressing UV-absorbing c-opsin1 have high resting calcium levels and show hyperpolarising and subsequent depolarising responses to UV light (405 nm) (Verasztó et al., 2018). In the present study, we have shown that the cells that strongly synapse with cPRCs are interneurons that specifically express NOS (INNOS). The fluorescence intensity of DAF-FM, which specifically detected INNOS, showed a transient tonic-like increase dependent on UV stimulation of the cPRCs. The graph shows a decrease in intensity after UV light is switched off, but the response of DAF-FM to NO is irreversible and this decrease is due to bleaching by the relatively strong excitation light. Attempts to measure changes in the intensity of the calcium indicator RGECO1a simultaneously with DAF-FM imaging did not lead to detection of changes in fluorescence intensity compared to GCaMP6s and could only visualise the cPRCs. In calcium imaging using GCaMP6s, INNOS identified by the positional relationship between the cPRC and INNOS and the labelling of RYamide depolarised in clear synchrony with the hyperpolarising response of the cPRCs. This tonic response may involve dopaminergic nerves based on single-cell data (**Figure 6**) [Puopolo et al. (2001)](Zhang et al., 2007)(Randel et al., 2014). In the mammalian retina, it is known that signals from bipolar photoreceptor cells are transmitted to downstream NOS-expressing amacrine cells (NOAC), where NO is produced (Jacoby et al., 2018). These suggest that UV stimulation of cPRCs causes the production of NO via a depolarising response of INNOS.

Our results suggest that NIT-GC1, which is specifically expressed in cPRCs, functions as a target for NO produced by INNOS and contributes to the regulation of the cPRC circuit transmission pathway via a depolarising response by increasing cGMP. In the mammalian retina, NO is an essential signalling molecule and one of the most well-

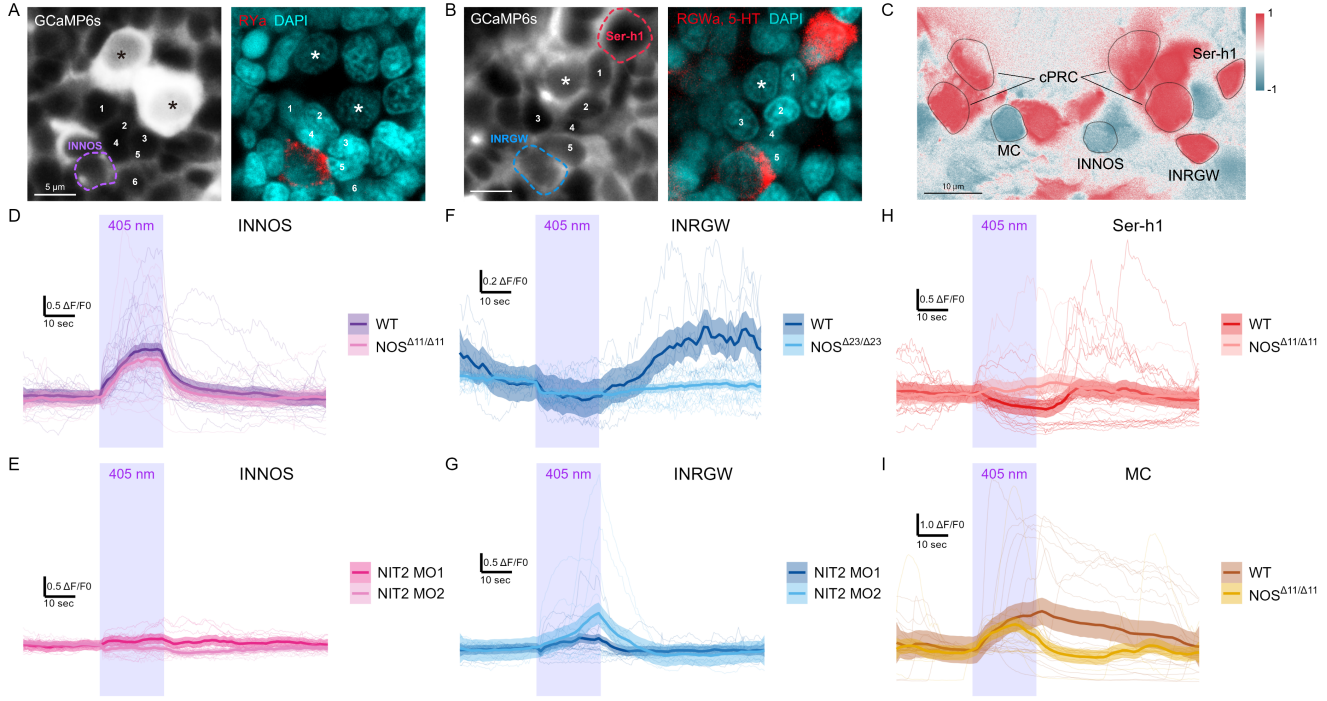


Figure 5: Figure 5. NO produced by UV stimulation to cPRCs induces a depolarising response in cPRCs via NIT-GC1. (A, B) Each left figure shows a calcium imaging using GCaMP6s. The respective right figures show immunostaining images of the same positions in the respective left figures, (A) shows RYamide antibodies, (B) shows RGWamide and serotonin (5-HT) antibodies in red and DAPI in cyan. Asterisks indicate the nuclei of the cPRC, respectively, and the nuclei of the cells that were identified from the arrangement of the surrounding cells are indicated by numbers. From the position of the cells, the calcium imaging data identify INNOS in (A) and INRGW and Ser-h1 in (B), respectively. **(C)** Correlation (Pearson's r) map of neuronal activity of the INNOS, INRGW, Ser-h1 and MC neurons. **(D)** Changes over time in GCaMP6s intensities in INNOS when cPRC is stimulated with UV in WT (dark purple) and $\text{NOS}^{\Delta 11/\Delta 11}$ mutant (light purple) larvae. **(E)** Changes over time in GCaMP6s intensities in INNOS when cPRC is stimulated with UV in NIT-GC2 morphants (MO1 and MO2: pink and light pink) larvae. **(F)** Changes over time in GCaMP6s intensities in INRGW when cPRC is stimulated with UV in WT (dark blue) and $\text{NOS}^{\Delta 23/\Delta 23}$ mutant (light blue) larvae. **(G)** Changes over time in GCaMP6s intensities in INRGW when cPRC is stimulated with UV in NIT-GC2 morphants (MO1 and MO2: blue and light blue). **(H, I)** Changes over time in GCaMP6s intensities in Ser-h1 and MC when cPRC is stimulated with UV in WT (Ser-h1 and MC: dark red and brown) and $\text{NOS}^{\Delta 11/\Delta 11}$ mutant (Ser-h1 and MC: light red and brown) larvae.

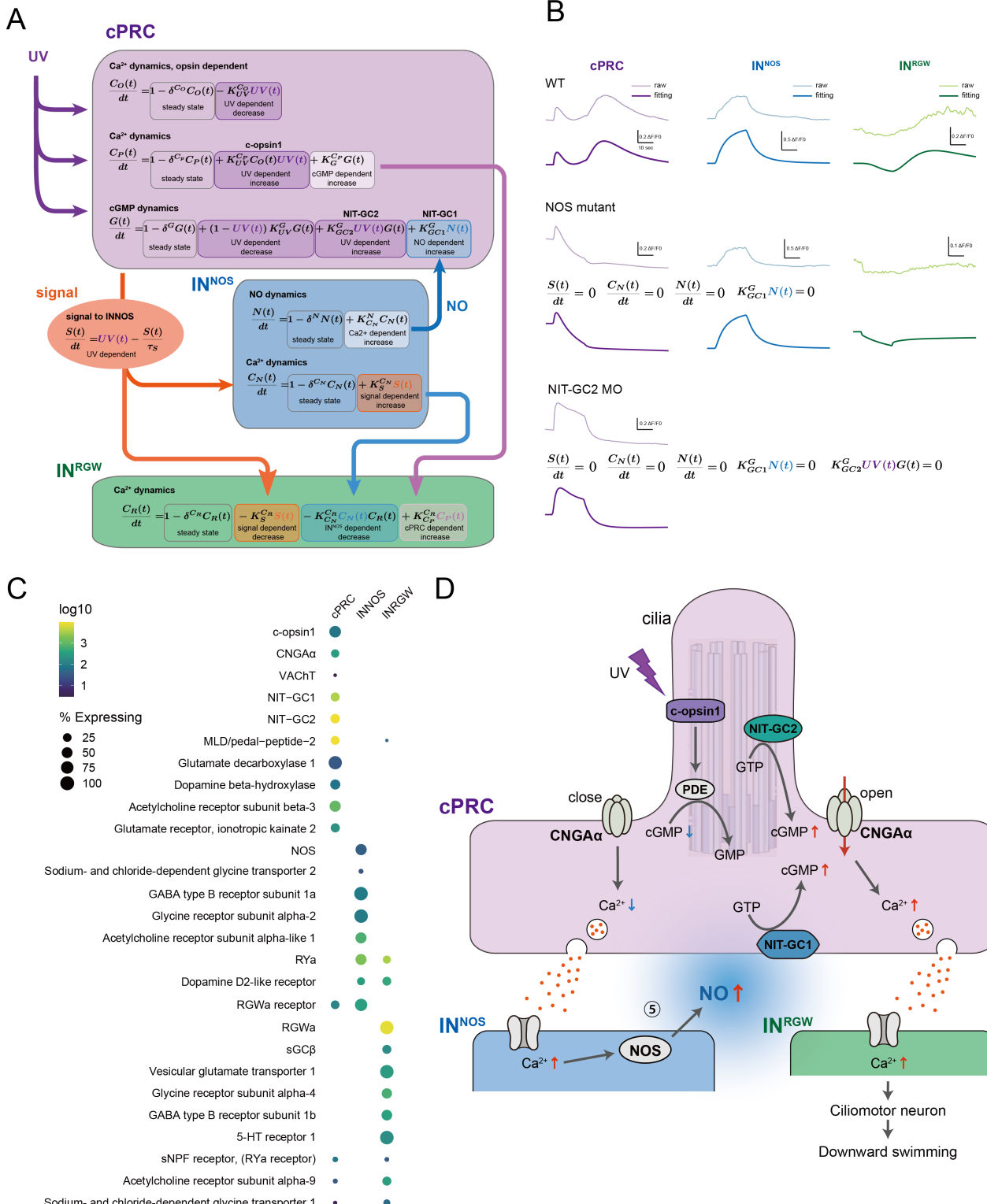


Figure 6: Figure 6. Gene expressions and signalling mechanisms between cPRC, INNOS and INRGWa. (C) Dot plot of genes (columns) expressed in three types of cells (rows) in the cPRC circuit using single cell RNA-Seq. The size of the dots is expressed in proportion to the percentage of cells expressing that gene relative to all cells. The colours represent the normal logarithm of the number of transcripts in the cells expressing the gene. **(D)** Schematic diagram of the signalling pathway of the cPRC circuit, focusing on the NO feedback.

studied (Cudeiro and Rivadulla, 1999). It has been reported that NO produced in one of the retinal cells modulates cGMP-mediated neurotransmission by activating presynaptic neural sGCs (general target of NO) through retrograde signalling [Vielma et al. (2014)](Wei et al., 2012). In Platynereis cPRC, NIT-GC1 was also identified as having the property of producing cGMP in a NO-dependent manner. Furthermore, it is known that CNGA α , one of the cyclic nucleotide-gated channels, is specifically highly expressed in cPRC (Tosches et al., 2014), and in INNOS-cPRC signalling, NO is implicated in the neuromodulation of the cPRC by retrograde signalling. NO is a molecule with a very short half-life, and when functioning as a signalling molecule, NOS and sGC are known to localise very close together at synapses between neurons [Burette et al. (2002)][Garthwaite, 2015]. In our study, we found 12 sGCs in Platynereis, but none expressed in the cPRC. Localisation analysis of NOS and NIT-GC1 by antibody staining showed that the two proteins localised very close together in the anterior neurosecretory plexus region. Calcium imaging results using NOS mutant and NIT-GC1 knockdown larvae suggest that NIT-GC1 activation induces a depolarising response in the cPRC.

Another type of interneuron that strongly synapses with the cPRC is the INRGWa, which synapses directly onto the ciliomotor neuron and is therefore considered to be a very important neuron in the control of larval behaviour [Verasztó et al. (2018)][Williams et al., 2017]. The present results suggest that the depolarising response of the cPRC due to NO feedback induces INRGW activation. RGWamide is also a neuropeptide that induces larval downward swimming quite strongly (unpublished? need to show data?), and the delayed downward swimming of NOS mutant larvae in response to UV stimulation may be responsible for the failure of INRGW activation to occur. In addition, in many marine invertebrates, NO has been reported to be involved in many aspects of settlement behaviour and metamorphosis induction (Bishop and Brandhorst, 2007, 2003; Castellano et al., 2014; Leise et al., 2001; Pechenik et al., 2007; Song et al., 2021; Ueda et al., 2016; Ueda and Degnan, 2014, 2013; Yang et al., 2018; Zhu et al., 2020). The downward swimming behaviour of Platynereis larvae is the first step in the onset of settlement behaviour and metamorphosis. These suggest that downward swimming due to NO activation of INRGWs may trigger the onset of settlement behaviour and metamorphosis [Conzelmann et al. (2013b)][Williams et al., 2015]. These suggest that NO feedback signalling may act as a trigger for downward swimming via activation of INRGWs, which induces the initiation of settlement behaviour and metamorphosis.

An outstanding question is how the NO~NIT-GC response alters neuronal dynamics. NO is a single molecule and, due to its short half-life, cannot be transmitted over long distances and has a limited signalling repertoire. It has therefore been considered unsuitable for generating diversity in signalling compared to other signalling molecules such as neuropeptides and classical neurotransmitters (Jékely, 2021). However, our results in the present study indicate that NO-induced activation of NIT-GC1 is involved in the regulation of neuronal circuits (cPRC pathway). The NIT domain was originally found in bacteria and the existence of GCs with NIT domains was first reported by Moroz et al in 2020 (Moroz et al., 2020; Shu et al., 2003). It has been proposed that NIT domains in bacteria regulate cellular functions in response to changes in extracellular and intracellular nitrate and/or nitrite concentrations (Camargo et al., 2007). In fact, NO is a free radical molecule, with a half-life of 5 msec in vivo, and is readily converted to nitrate and nitrite (Garthwaite, 2015; Möller et al., 2019; Santos et al., 2011). And nitrate and nitrite have been reported to accumulate in cells and tissues with high NOS activity in placozoans and cnidarians (Moroz et al., 2020, 2004). It is possible that the NIT domains of NIT-GC1 identified in this study may also be used for nitrate/nitrite sensing, as in bacteria. Furthermore, if they show different sensitivities to NO, nitrite and nitrate, it is possible that the temporal variation in their respective half-lives could give rise to a repertoire of activation timings (Lundberg et al., 2011). In addition, we have found at least 15 NIT-GCs in the Platynereis transcriptome data, of which NIT-GC2 is highly expressed in the cPRC, in addition to NIT-GC1. Interestingly, NIT-GC2 showed a very different localisation pattern to NIT-GC1, and furthermore, the results of calcium imaging of cPRC in response to UV stimulation using NIT-GC2 knockdown larvae were the different dynamics (such that hyperpolarisation was suppressed) with NIT-GC1 knockdown. It was not clear from the present analysis whether this difference was due to differences in the localisation or the property of the NIT-GCs. However, the diversification and spatially different localisation patterns of NIT-GCs may increase their signalling repertoire. We also believe that the appearance of NIT-GCs was one of the means to generate the diversity of signalling pathways using NO during the early stages of

nervous system evolution in metazoans, since sponges and ctenophores, where NO signalling is present, have no NIT-GCs at all, as many as 12 have been found in placozoans, and NIT-GCs are functional in the “proto-eye” circuit of Platynereis.

Materials and Methods

CRISPR-Cas9 Design and Microinjection

Before designing the small guide RNA (sgRNA) for the sgRNA:Cas9 nuclease, splice sites and polymorphic sites in our laboratory culture were identified to avoid them. The sgRNA targeted the third exon of *Platynereis dumerilii* NOS (target site: 5'-GGGCAATACTGGCTCCACTC-3'). The sgRNA was assembled from two annealed oligonucleotides (5'-TAGGGCAATACTGGCTCCACTC-3', 5'-AAACGAGTGGAGCCAGTATTGC-3') forming overhangs for cloning into a Bsal site of the plasmid pDR27456 (Hwang et al. 2013)(42250, Addgene), which contains next to the Bsal site a tracrRNA sequence. The plasmid was then used to PCR amplify DNA (primers: T7, 5'-AAAAGCACCGACTCGGTGCC-3') for synthesizing the sgRNA. The DNA was purified with the QIAquick PCR Purification Kit (Qiagen). From the DNA, the sgRNA was synthesized with the MEGAshortscript Kit (Thermo Fisher Scientific) and was purified with the MEGAclear Kit (Thermo Fisher Scientific). Cas9-mRNA was transcribed, capped, and polyA-tailed with the mMessage mMachine Kit and the Poly(A) Tailing Kit (both Thermo Fisher Scientific) from a plasmid (pUC57-T7-RPP2-Cas9) containing the Cas9 ORF fused to 169 base pair 5' UTR from the *Platynereis dumerilii* 60S acidic ribosomal protein P2. The sgRNA (18 ng/ml) and the Cas9-mRNA (180 ng/μl) were coinjected into fertilized eggs of *Platynereis dumerilii* wild-type parents according to an established injection procedure (Conzelmann et al., 2013a). The eggs were kept at 18°C for 45 min before injection and were injected at 14.5°C. The injected individuals were kept at 18°C for 5 to 8 days in 6-well- plates (Nunc multidish no. 150239, Thermo Scientific) and then cultured at 22°C until sexual maturity. The mature worms were crossed to wild-type worms and the progeny was genotyped, resulting in two founder lines, which were bred to homozygosity.

NOS sequencing and genotyping

For genotyping of the NOS locus, genomic DNA was isolated from single larvae, groups of 6-20 larvae, or from the tails of adult worms. The DNA was amplified by PCR (primers: 5'-GGTCATTGGTTTCGATAACATTGCGG-3', 5'-CAGAGTCGATCAGTCTGCATATCTCCA-3') with the dilution protocol of the Phusion Human Specimen Direct PCR Kit (Thermo Scientific). The PCR product was sequenced directly with a nested sequencing primer (5'-GGTGCTCTCCGGGTACACAA-3'). A mixture of wild-type and deletion alleles in a sample gave double peaks in the sequencing chromatograms, with the relative height of the double peaks reflecting the relative allele ratio in the sample.

Vertical column setup for measuring photoresponses

Photoresponses of larvae of different ages were assayed in a vertical Plexiglas column (31 mm x 10 mm x 160 mm water height). The column was illuminated from top with light from a monochromator (Polychrome II, Till Photonics). The monochromator was controlled by AxioVision 4.8.2.0 (Carl Zeiss MicroImaging GmbH) via analog voltage. The light passed a collimator lens (LAG-65.0-53.0-C with MgF₂ Coating, CVI Melles Griot) before entering the column. The column was illuminated from both sides with light-emitting diodes (LEDs). The LEDs on each side were grouped into two strips. One strip contained UV (395 nm) LEDs (SMB1W-395, Roithner Lasertechnik) and the other infrared (810 nm) LEDs (SMB1W-810NR-I, Roithner Lasertechnik). The UV LEDs were run at 4 V to stimulate the larvae in the column from the side. The infrared LEDs were run at 8 V (overvoltage) to illuminate the larvae for the camera (DMK 22BUC03, The Imaging Source), which recorded videos at 15 frames per second and was controlled by IC Capture (The Imaging Source).

Comparing behavior of wildtype and NOS-knockout 3-day-old larvae

To compare the behavior of wildtype and NOS-knockout larvae at 3 days in the vertical column, the larvae were mixed and left in the dark for 5 min. The larvae were treated with NOS inhibitors for pharmacology. The NOS inhibitors

were L-NAME. The larvae were treated with different concentrations in adjacent columns. The concentrations for the NOS inhibitors were control, 1 mM, 0.1 mM. The larvae were recorded for 1 min in the dark followed by exposure to collimated cyan (480 nm) light from the top of the column for 2 min, then 2 min darkness, and finally collimated UV (395 nm) light from the top of the column for 2 min. Stimulus light was provided by the monochromator (Polychrome II, Till Photonics). Scripts are available at <https://github.com/JekelyLab/NOS>.

NOS Identification and Phylogenetic Analysis

To identify NOS, we obtained a “seed” database of oxygenase domain in Pfam database, PF02898. From these sequences, we produced a Hidden Markov Model (HMM) and used this to mine the 47 metazoan species, 2 choanoflagellate species and 2 filasterea species investigated. HMM models were run in HMMR3 with an e-value of 1e-15. We ran CD-Hit (Fu et al., 2012) to eliminate redundant sequences (at a 80% threshold). We aligned the sequences with MAFFT version 7, with the iterative refinement method E-INS-i. Alignments were trimmed with TrimAI in gappy-out mode (Capella-Gutierrez et al., 2009). To calculate maximum-likelihood trees, we used IQ-tree2 with the LG+G4 model. To calculate branch support, we ran 1,000 replicates with the aLRT-SH-like and aBayes methods (Minh et al., 2020). The sequences used for the phylogenetic analysis are available in **Supplementary File 2**, the trimmed alignment is available in **Supplementary File 3**.

NIT-GC Identification and Phylogenetic Analysis

To identify NIT-GCs, we obtained a “seed” database of Adenylate and Guanylate cyclase catalytic domain in Pfam database, PF00211. From these sequences, we produced a Hidden Markov Model (HMM) and used this to mine the 45 metazoan species, 2 choanoflagellate species and 2 filasterea species investigated. HMM models were run in HMMR3 with an e-value of 1e-15. We ran CD-Hit (Fu et al., 2012) to eliminate redundant sequences (at a 80% threshold). The CLANS analysis is available as **Supplementary File 1**. To identify clusters, we used the convex-clustering option with 100 jack-knife replicates. The NIT-GCs are extremely well conserved in membrane-bound guanylate cyclases and form an easily recognizable cluster. To analyze the phylogeny of NIT-GCs, the cluster containing these GCs together with membrane-bound guanylate cyclases were parsed and used for tree building. We aligned the sequences with MAFFT version 7, with the iterative refinement method E-INS-i. Alignments were trimmed with TrimAI in gappy-out mode (Capella-Gutierrez et al., 2009). To calculate maximum-likelihood trees, we used IQ-tree2 with the LG+G4 model. To calculate branch support, we ran 1,000 replicates with the aLRT-SH-like and aBayes methods (Minh et al., 2020). The sequences used for the phylogenetic analysis are available in **Supplementary File 2**, the trimmed alignment is available in **Supplementary File 3**.

Single-cell analysis

We used Achim et al. for the single-cell data (Achim et al., 2015). In fact, in Williams et al., they used 107 cells as neurons by removing duplicates from Achim et al. single-cell data, so we used those cells (Williams et al., 2017). Since the raw data were read count data, we normalized them to TPM using Python. After that we converted them to log10. From the sum of the expression levels in 107 cells for each gene, I calculated the percentage in each cell. We chose the appropriate genes for now. For each cell, we identified them with marker genes. After created the data in Python, plotted it using R dot plots. RPKM calculates the total number of reads per million bp and then divides by the length of each gene, so it is not possible to compare between samples. Instead, TPM first divides by the length of the gene and then divides by the total number of reads per million bases, which allows for more accurate comparisons between samples. In this case we wanted to compare between samples, so we used TPM. In fact, TPM is becoming the mainstream method for many single-cell analyses. The total TPM of each gene between the samples was used to calculate the percentage of expressed genes.

In situ HCR

Larvae were fixed and treated with Proteinase K, according to the conventional WMISH protocol (Tessmar-Raible et al., 2005), with fixation in 4% paraformaldehyde/ PTW (PBS with 0.05% Tween20) for 2 hr at room temperature, and Proteinase K treatment in 100 µg/ml Proteinase K/ PTW for 3 min (Tessmar-Raible et al., 2005). Specifically,

for the HCR protocol, samples were processed in 1.5 ml tubes. Probe hybridization buffer, probe wash buffer, amplification buffer, and fluorescent HCR hairpins were purchased from Molecular Instruments (Los Angeles, USA). Hairpins associated with the b2 initiator sequence were labeled with Alexa Fluor 647, and the hairpins associated with the b3 initiator sequence were labeled with Alexa Fluor 546. To design probes for HCR, we used custom software (Kuehn et al., 2021) to create 20 DNA oligo probe pairs specific to *P. dumerilii* NOS, NIT-GC1, NIT-GC2, RYα-pNP (GenBank accession: JF811330.1), c-opsin1 (GenBank accession: AY692353.1), CNGAα (GenBank accession: KM199644.1), and MLD/pedal2-pNP (GenBank accession: KF515945.1). The NOS, NIT-GC1 and NIT-GC2 probes were designed to be associated with the b2 initiator sequence, while the RYα-pNP, c-opsin1, CNGAα and MLD/pedal2-pNP probes were designed to be associated with the b3 initiator sequence. For the detection stage, samples were pre-hybridized in 200 µl of probe hybridization buffer for 1 hr at 37°C, and then incubated in 250 µl hybridization buffer containing probe oligos (4 pmol/ml) overnight at 37°C. To remove excess probe, samples were washed 4× with 1 ml hybridization wash buffer for 15 min at 37°C, and subsequently 2× in 1 ml 5× SSCT (5× SSC with 0.1% Tween20) for 5 min at room temperature. For the amplification stage, samples were pre-incubated with 100 µl of amplification buffer for 30 min, room temperature, and then incubated with 150 µl amplification buffer containing fluorescently labeled hairpins (40nM concentration (2ul of 3uM stock in 150ul amplification buffer, snap-cooled as described; (Choi et al., 2018)) overnight in the dark at 25°C. To remove excess hairpins, samples were washed in 1 ml 5× SSCT at room temperature, twice for 5 min, twice for 30 min, and once for 5 min. During the first 30 min wash, samples were counterstained with DAPI (Cat. #40043, Biotium, USA).

Immunohistochemistry

Whole-mount immunostaining of 2 day old *Platynereis* larvae fixed with 4% paraformaldehyde were carried out using primary antibodies raised against NIT-GC1, NIT-GC2, NOS, RYamide neuropeptide, RGWamide neuropeptide in rabbit, plus a commercial antibody raised against acetylated tubulin in mouse (Sigma T7451). The synthetic peptides contained an N-terminal Cys that was used for coupling during purification. Antibodies were affinity purified from sera as previously described (Conzelmann and Jékely, 2012). Immunostainings were carried out as previously described (Conzelmann and Jékely, 2012). The NOS promoter (fragment sizes: 12 Kb) was amplified and cloned upstream of 3xHA- Palmito-tdTomato. Larvae injected with promoter constructs (ca. 250 ng/ml) were analysed for reporter expression at 3 days post fertilization using an AxioImager Z.1 fluorescence wide-field microscope (Carl Zeiss GmbH, Jena) and immediately fixed for immunostainings. The protocol followed for immunostaining of HA-tagged reporters was recently described (Verasztó et al., 2017). Specimens were imaged with a LSM 780 NLO or LSM 880 with Airysan Confocal Microscope (Zeiss, Jena).

Calcium imaging

For calcium imaging, 49–55 hpf larvae were used. Experiments were performed at room temperature and larvae were immobilised by being embedded in 2.5% agarose filtered artificial seawater between a slide and coverslip spaced with adhesive tape. GCaMP6s mRNA (1 mg/ml) was injected into zygotes as described previously (Randel et al., 2014). Larvae were imaged on a Zeiss LSM 880 with Airyscan (with a C-Apochromat 63X/1.2 Corr - water) with a frame rate of 1.88 frame/sec and an image size of 512 x 512 pixels. The larvae were stimulated in a region of interest (a circle with ?? pixel diameter) with 405 nm lasers controlled by the Bleaching mode. The imaging laser had a similar intensity than the stimulus laser but covered an area that was 10 times larger than the stimulus ROI.

Cell culture experiment

Green cGull was used for the cGMP assay (Matsuda et al., 2016). A full-length Pdum-NIT-GC1 and -NIT-GC2 coding sequences were amplified by PCR starting from a *Platynereis dumerilii* cDNA library and cloned into the pcDNA3.1(+) vector using the T2A self-cleaving sequence. Cos-7 cells with low expression of endogenous soluble guanylate cyclase were used as cultured cells for gene expression. This cell line was purchased from Angio-proteomie (CAT no. cAP-0203). The Cos-7 cells were maintained at 37 °C in 35mm dishes (Nunc™ Glass Bottom Dishes) containing 3 mL of DMEM, high glucose glutamax medium (Thermo; Cat. No. 10566016) supplemented with 10% fetal bovine serum (Thermo; Cat. No. 10082147). Upon reaching confluence of approximately 85%, we

transfected the cells with the plasmid containing Green cGull-T2A-NITGC1. Transfections were carried out with 150 ng of each plasmid and 0.3 µl of the transfection Lipofectamine 3000 Reagent (invitrogen; Cat. No. L3000001). Two days post-transfection, we removed the culture medium and substituted it for fresh DMEM-medium. For single-wavelength imaging experiments, cells in 35-mm dishes were washed twice and imaged in modified Ringer's buffer (140 mM NaCl, 3.5 mM KCl, 0.5mM NaH₂PO₄, 0.5mM S-3 MgSO₄, 1.5 mM CaCl₂, 10 mM HEPES, 2 mM NaHCO₃ and 5 mM glucose). Dishes were mounted on a stage heated at 37 °C and imaging was performed using an inverted microscope (LSM880, Zeiss) equipped with an oil-immersion objective lens (UAp0/340, 40×, NA = xx). Images were acquired using a xenon lamp, 460–495 nm excitation filter, 505-nm dichroic mirror and 510– 550-nm emission filter (????). S-Nitroso-N-acetyl-D, L-penicillamine (SNAP) was purchased from Sigma-Aldrich (St. Louis, MO, USA). The exposure time of the EM-CCD camera was controlled by the ZEN software (Zeiss). Images were acquired every 15 s for 10 min and stimulation was initiated 2 min after starting image acquisition. Imaging data analysis was performed using ImageJ (National Institutes of Health, Bethesda, MD, USA).

Acknowledgements

This work was funded by the Wellcome Trust (214337/Z/18/Z).

References

- Achim K, Pettit J-B, Saraiva LR, Gavriouchkina D, Larsson T, Arendt D, Marioni JC. 2015. High-throughput spatial mapping of single-cell RNA-seq data to tissue of origin. *Nature Biotechnology* **33**:503–509. doi:10.1038/nbt.3209
- Arendt D, Tessmar-Raible K, Snyman H, Dorresteijn AW, Wittbrodt J. 2004. Ciliary Photoreceptors with a Vertebrate-Type Opsin in an Invertebrate Brain. *Science* **306**:869–871. doi:10.1126/science.1099955
- Bishop CD, Brandhorst BP. 2007. Development of nitric oxide synthase-defined neurons in the sea urchin larval ciliary band and evidence for a chemosensory function during metamorphosis. *Developmental Dynamics* **236**:1535–1546. doi:10.1002/dvdy.21161
- Bishop CD, Brandhorst BP. 2003. On nitric oxide signaling, metamorphosis, and the evolution of biphasic life cycles. *Evolution and Development* **5**:542–550. doi:10.1046/j.1525-142x.2003.03059.x
- Burette A, Zabel U, Weinberg RJ, Schmidt HHW, Valtschanoff JG. 2002. Synaptic Localization of Nitric Oxide Synthase and Soluble Guanylyl Cyclase in the Hippocampus. *The Journal of Neuroscience* **22**:8961–8970. doi:10.1523/jneurosci.22-20-08961.2002
- Camargo A, Llamas A, Schnell RA, Higuera JoseJ, González-Ballester D, Lefebvre PA, Fernández E, Galván A. 2007. Nitrate Signaling by the Regulatory Gene *NIT2* in *Chlamydomonas*. *The Plant Cell* **19**:3491–3503. doi:10.1105/tpc.106.045922
- Capella-Gutierrez S, Silla-Martinez JM, Gabaldon T. 2009. trimAl: a tool for automated alignment trimming in large-scale phylogenetic analyses. *Bioinformatics* **25**:1972–1973. doi:10.1093/bioinformatics/btp348
- Castellano I, Ercoles E, Palumbo A. 2014. Nitric Oxide Affects ERK Signaling through Down-Regulation of MAP Kinase Phosphatase Levels during Larval Development of the Ascidian *Ciona intestinalis*. *PLoS ONE* **9**:e102907. doi:10.1371/journal.pone.0102907
- Choi HMT, Schwarzkopf M, Fornace ME, Acharya A, Artavanis G, Stegmaier J, Cunha A, Pierce NA. 2018. Third-generation *in situ* hybridization chain reaction: multiplexed, quantitative, sensitive, versatile, robust. *Development* **145**. doi:10.1242/dev.165753
- Conzelmann M, Jékely G. 2012. Antibodies against conserved amidated neuropeptide epitopes enrich the comparative neurobiology toolbox. *EvoDevo* **3**:23. doi:10.1186/2041-9139-3-23
- Conzelmann M, Offenburger S-L, Asadulina A, Keller T, Münch TA, Jékely G. 2011. Neuropeptides regulate swimming depth of *Platynereis* larvae. *Proceedings of the National Academy of Sciences* **108**. doi:10.1073/pnas.1109085108
- Conzelmann M, Williams Elizabeth A, Krug K, Franz-Wachtel M, Macek B, Jékely G. 2013a. The neuropeptide complement of the marine annelid *Platynereis dumerilii*. *BMC Genomics* **14**:906. doi:10.1186/1471-2164-14-906
- Conzelmann M, Williams Elizabeth A, Tunaru S, Randel N, Shahidi R, Asadulina A, Berger J, Offermanns S, Jékely

- G. 2013b. Conserved MIP receptor–ligand pair regulates *Platynereis* larval settlement. *Proceedings of the National Academy of Sciences* **110**:8224–8229. doi:10.1073/pnas.1220285110
- Cudeiro J, Rivadulla C. 1999. Sight and insight – on the physiological role of nitric oxide in the visual system. *Trends in Neurosciences* **22**:109–116. doi:10.1016/s0166-2236(98)01299-5
- Fu L, Niu B, Zhu Z, Wu S, Li W. 2012. CD-HIT: accelerated for clustering the next-generation sequencing data. *Bioinformatics* **28**:3150–3152. doi:10.1093/bioinformatics/bts565
- Garthwaite J. 2015. From synaptically localized to volume transmission by nitric oxide. *The Journal of Physiology* **594**:9–18. doi:10.1113/jp270297
- Jacoby J, Nath A, Jessen ZF, Schwartz GW. 2018. A Self-Regulating Gap Junction Network of Amacrine Cells Controls Nitric Oxide Release in the Retina. *Neuron* **100**:1149–1162.e5. doi:10.1016/j.neuron.2018.09.047
- Jékely G. 2021. The chemical brain hypothesis for the origin of nervous systems. *Philosophical Transactions of the Royal Society B: Biological Sciences* **376**:20190761. doi:10.1098/rstb.2019.0761
- Kuehn E, Clausen DS, Null RW, Metzger BM, Willis AD, Özpolat BD. 2021. Segment number threshold determines juvenile onset of germline cluster expansion in *Platynereis dumerilii*. *Journal of Experimental Zoology Part B: Molecular and Developmental Evolution* **338**:225–240. doi:10.1002/jez.b.23100
- Leise EM, Thavaradhara K, Durham NR, Turner BE. 2001. Serotonin and Nitric Oxide Regulate Metamorphosis in the Marine Snail *Lymanassa obsoleta*. *American Zoologist* **41**:258–267. doi:10.1093/icb/41.2.258
- Lundberg JO, Weitzberg E, Shiva S, Gladwin MT. 2011. The nitrate–nitrite–nitric oxide pathway in mammals. Humana Press. pp. 21–48. doi:10.1007/978-1-60761-616-0_3
- Matsuda S, Harada K, Ito M, Takizawa M, Wongso D, Tsuboi T, Kitaguchi T. 2016. Generation of a cGMP Indicator with an Expanded Dynamic Range by Optimization of Amino Acid Linkers between a Fluorescent Protein and PDE5? *ACS Sensors* **2**:46–51. doi:10.1021/acssensors.6b00582
- Minh BQ, Schmidt HA, Chernomor O, Schrempf D, Woodhams MD, Haeseler A von, Lanfear R. 2020. IQ-TREE 2: New Models and Efficient Methods for Phylogenetic Inference in the Genomic Era. *Molecular Biology and Evolution* **37**:1530–1534. doi:10.1093/molbev/msaa015
- Möller MN, Rios N, Trujillo M, Radi R, Denicola A, Alvarez B. 2019. Detection and quantification of nitric oxide–derived oxidants in biological systems. *Journal of Biological Chemistry* **294**:14776–14802. doi:10.1074/jbc.rev119.006136
- Monteagudo-Cascales E, Ortega Á, Velando F, Morel B, Matilla MA, Krell T. 2023. Study of NIT domain-containing chemoreceptors from two global phytopathogens and identification of NIT domains in eukaryotes. *Molecular Microbiology*. doi:10.1111/mmi.15069
- Moroz LL, Meech RW, Sweedler JV, Mackie GO. 2004. Nitric oxide regulates swimming in the jellyfish *Aglantha digitale*. *The Journal of Comparative Neurology* **471**:26–36. doi:10.1002/cne.20023
- Moroz LL, Romanova DY, Nikitin MA, Sohn D, Kohn AB, Neveu E, Varoqueaux F, Fasshauer D. 2020. The diversification and lineage-specific expansion of nitric oxide signaling in Placozoa: insights in the evolution of gaseous transmission. *Scientific Reports* **10**. doi:10.1038/s41598-020-69851-w
- Ozpolat BD, Randel N, Williams EA, Bezires-Calderón LA, Andreatta G, Balavoine G, Bertucci PY, Ferrier DEK, Gambi MC, Gazave E, Handberg-Thorsager M, Hardege J, Hird C, Hsieh Y-W, Hui J, Mutemi KN, Schneider SQ, Simakov O, Vergara HM, Vervoort M, Jékely G, Tessmar-Raible K, Raible F, Arendt D. 2021. The Nereid on the rise: *Platynereis* as a model system. *Zenodo*. doi:10.5281/ZENODO.4907400
- Pechenik JA, Cochrane DE, Li W, West ET, Pires A, Leppo M. 2007. Nitric Oxide Inhibits Metamorphosis in Larvae of *Crepidula fornicata*, the Slippershell Snail. *The Biological Bulletin* **213**:160–171. doi:10.2307/25066632
- Puopolo M, Hochstetler SE, Gustincich S, Wightman RM, Raviola E. 2001. Extrasynaptic Release of Dopamine in a Retinal Neuron. *Neuron* **30**:211–225. doi:10.1016/s0896-6273(01)00274-4
- Randel N, Asadulina A, Bezires-Calderón LA, Verasztó C, Williams EA, Conzelmann M, Shahidi R, Jékely G. 2014. Neuronal connectome of a sensory-motor circuit for visual navigation. *eLife* **3**. doi:10.7554/elife.02730
- Santos RM, Lourenço CF, Pomerleau F, Huettl P, Gerhardt GA, Laranjinha J, Barbosa RM. 2011. Brain Nitric Oxide Inactivation Is Governed by the Vasculature. *Antioxidants & Redox Signaling* **14**:1011–1021. doi:10.1089/ars.2010.3297
- Shu CJ, Ulrich LE, Zhulin IB. 2003. The NIT domain: a predicted nitrate-responsive module in bacterial sensory

- receptors. *Trends in Biochemical Sciences* **28**:121–124. doi:10.1016/s0968-0004(03)00032-x
- Song H, Hewitt OH, Degnan SM. 2021. Arginine Biosynthesis by a Bacterial Symbiont Enables Nitric Oxide Production and Facilitates Larval Settlement in the Marine-Sponge Host. *Current Biology* **31**:433–437.e3. doi:10.1016/j.cub.2020.10.051
- Tessmar-Raible K, Steinmetz PRH, Snyman H, Hassel M, Arendt D. 2005. Fluorescent two-color whole mount *in situ* hybridization in *Platynereis dumerilii* (Polychaeta, Annelida), an emerging marine molecular model for evolution and development. *BioTechniques* **39**:460–464. doi:10.2144/000112023
- Tosches M, Bucher D, Vopalensky P, Arendt D. 2014. Melatonin Signaling Controls Circadian Swimming Behavior in Marine Zooplankton. *Cell* **159**:46–57. doi:10.1016/j.cell.2014.07.042
- Tsukamoto H, Chen I-S, Kubo Y, Furutani Y. 2017. A ciliary opsin in the brain of a marine annelid zooplankton is ultraviolet-sensitive, and the sensitivity is tuned by a single amino acid residue. *Journal of Biological Chemistry* **292**:12971–12980. doi:10.1074/jbc.m117.793539
- Ueda N, Degnan SM. 2014. Nitric oxide is not a negative regulator of metamorphic induction in the abalone *haliotis asinina*. *Frontiers in Marine Science* **1**. doi:10.3389/fmars.2014.00021
- Ueda N, Degnan SM. 2013. Nitric Oxide Acts as a Positive Regulator to Induce Metamorphosis of the Ascidian *Herdmania momus*. *PLoS ONE* **8**:e72797. doi:10.1371/journal.pone.0072797
- Ueda N, Richards GS, Degnan BM, Kranz A, Adamska M, Croll RP, Degnan SM. 2016. An ancient role for nitric oxide in regulating the animal pelagobenthic life cycle: evidence from a marine sponge. *Scientific Reports* **6**. doi:10.1038/srep37546
- Veedin Rajan VB, Häfker NS, Arboleda E, Poehn B, Gossenreiter T, Gerrard E, Hofbauer M, Mühlstein C, Bileck A, Gerner C, Ribera d'Alcalá M, Buia MC, Hartl M, Lucas RJ, Tessmar-Raible K. 2021. Seasonal variation in UVA light drives hormonal and behavioural changes in a marine annelid via a ciliary opsin. *Nature Ecology & Evolution* **5**:204–218. doi:10.1038/s41559-020-01356-1
- Verasztó C, Gühmann M, Jia H, Rajan VBV, Bezires-Calderón LA, Piñeiro-Lopez C, Randel N, Shahidi R, Michiels NK, Yokoyama S, Tessmar-Raible K, Jékely G. 2018. Ciliary and rhabdomeric photoreceptor-cell circuits form a spectral depth gauge in marine zooplankton. *eLife* **7**. doi:10.7554/elife.36440
- Verasztó C, Jasek S, Gühmann M, Shahidi R, Ueda N, Beard JD, Mendes S, Heinz K, Bezires-Calderón LA, Williams E, Jékely G. 2020. Whole-animal connectome and cell-type complement of the three-segmented *Platynereis dumerilii* larva.
- Verasztó C, Ueda N, Bezires-Calderón LA, Panzera A, Williams EA, Shahidi R, Jékely G. 2017. Ciliomotor circuitry underlying whole-body coordination of ciliary activity in the *Platynereis* larva. *eLife* **6**. doi:10.7554/elife.26000
- Vielma AH, Agurto A, Valdés J, Palacios AG, Schmachtenberg O. 2014. Nitric Oxide Modulates the Temporal Properties of the Glutamate Response in Type 4 OFF Bipolar Cells. *PLoS ONE* **9**:e114330. doi:10.1371/journal.pone.0114330
- Wei T, Schubert T, Paquet-Durand F, Tanimoto N, Chang L, Koeppen K, Ott T, Griesbeck O, Seeliger MW, Euler T, Wissinger B. 2012. Light-Driven Calcium Signals in Mouse Cone Photoreceptors. *Journal of Neuroscience* **32**:6981–6994. doi:10.1523/jneurosci.6432-11.2012
- Williams EA, Conzelmann M, Jékely G. 2015. Myoinhibitory peptide regulates feeding in the marine annelid *Platynereis*. *Frontiers in Zoology* **12**. doi:10.1186/s12983-014-0093-6
- Williams EA, Verasztó C, Jasek S, Conzelmann M, Shahidi R, Bauknecht P, Mirabeau O, Jékely G. 2017. Synaptic and peptidergic connectome of a neurosecretory center in the annelid brain. *eLife* **6**. doi:10.7554/elife.26349
- Yang X-X, Wong YH, Zhang Y, Zhang G, Qian P-Y. 2018. Exploring the regulatory role of nitric oxide (NO) and the NO-p38MAPK/cGMP pathway in larval settlement of the bryozoan *Bugula neritina*. *Biofouling* **34**:545–556. doi:10.1080/08927014.2018.1470240
- Zhang D-Q, Zhou T-R, McMahon DG. 2007. Functional Heterogeneity of Retinal Dopaminergic Neurons Underlying Their Multiple Roles in Vision. *Journal of Neuroscience* **27**:692–699. doi:10.1523/jneurosci.4478-06.2007
- Zhu Y-T, Zhang Y, Liu Y-Z, Li Y-F, Yoshida A, Osatomi K, Yang J-L, Liang X. 2020. Nitric oxide negatively regulates larval metamorphosis in hard-shelled mussel (*mytilus coruscus*). *Frontiers in Marine Science* **7**.

